Received: 20 July 2018 | Revised: 26 May 2019 | Accepted: 21 August 2019

DOI: 10.1111/clr.13532

ORIGINAL RESEARCH

CLINICAL ORAL IMPLANTS RESEARCH WILEY

Effect of platelet-rich plasma on peri-implant trabecular bone volume and architecture: A preclinical micro-CT study in beagle dogs

Yan Huang[1,2] | Zhaokai Li[3] | Jeroen Van Dessel[2] | Benjamin Salmon[4] | Bo Huang[5] | Ivo Lambrichts[6] | Constantinus Politis[2] | Reinhilde Jacobs[2,7]

[1]West China College of Stomatology, State Key Laboratory of Oral Diseases & National Clinical Research Center for Oral Diseases, Sichuan University, Chengdu, China

[2]Department of Imaging & Pathology, Faculty of Medicine, OMFS IMPATH Research Group, KU Leuven and Oral and Maxillofacial Surgery, University Hospitals Leuven, Leuven, Belgium

[3]Department of Geriatric Medicine & National Clinical Research Center for Geriatric Disorders, Xiangya Hospital, Central South University, Changsha, Hunan, China

[4]Paris Descartes University - Sorbonne Paris Cité, EA 2496 - Orofacial Pathologies, Imaging and Biotherapies Lab and Dental Medicine Department, Bretonneau Hospital, HUPNVS, AP-HP, Paris, France

[5]Implant Center, West China College of Stomatology, Sichuan University, Chengdu, China

[6]Group of Morphology, Biomedical Research Institute, Hasselt University, Diepenbeek, Belgium

[7]Department of Dental Medicine, Karolinska Institutet, Stockholm, Sweden

Correspondence
Reinhilde Jacobs, Department of Imaging & Pathology, OMFS IMPATH Research Group, University of Leuven, Kapucijnenvoer 33, B3000 Leuven, Belgium.
Email: reinhilde.jacobs@kuleuven.be

Funding information
Sichuan Province Science and Technology Support Program, Grant/Award Number: 2016SZ0010; Fonds Wetenschappelijk Onderzoek, Grant/Award Number: 11. ZU.117N

Abstract

Objectives: To evaluate the peri-implant trabecular bone volume and architecture changes with 6-month follow-up after local application of platelet-rich plasma (PRP) and platelet-poor plasma (PPP) using high-resolution micro-CT.

Material and methods: Seventy-two dental implants were placed into healed mandibular sites of 9 beagle dogs. Implants were randomly divided into 4 groups following a split-mouth design: control I; control II; PPP; and PRP. Primary and secondary stabilities were assessed using resonance frequency analyses. At 1, 3, and 6 months after implant loading, trabecular structural parameters were evaluated at 0.5, 1, and 1.5 mm away from implants using micro-CT (voxel = 20 μm).

Results: Primary and secondary stabilities were equivalent in all conditions. PPP and PRP groups showed higher bone volume fraction (BV/TV) and trabecular thickness (Tb.Th) but lower trabecular separation (Tb.Sp) and total porosity percentage (Po (tot)) at all 3 time points. A significant decrease in BV/TV and Tb.Th was found for the control groups after 3 months of healing, while this was not observed in both the PPP and PRP groups. However, no distinct difference was found between the PRP and PPP groups over time. Moreover, as the investigated distance from the implant surface increased, BV/TV and Po (tot) within the same group and time point stayed the same, yet Tb.Th and Tb.Sp continued to increase.

Conclusions: Platelet-rich plasma and PPP with conventional implant placement lead to similar primary and secondary implant stability, but improved peri-implant bone volume and structural integration. The present research does not seem to suggest a different bone remodeling pattern when using PRP or PPP.

KEYWORDS

animal model, dental implants, dogs, guided tissue regeneration, micro-CT, morphometric analysis, platelet-rich plasma

1 | INTRODUCTION

Bone grafting is typically employed to restore bone defects and satisfy osseointegration of dental implants. Since the past decade, autologous products derived from blood centrifugation, such as platelet-rich plasma (PRP), have gained attention in regenerative medicine, including orthopaedics, cardiovascular surgery, cosmetics, urology, and especially in oral and maxillofacial surgery (Buser, Sennerby, & De Bruyn, 2017; Roffi, Filardo, Elizaveta, & Marcacci, 2013; Sampson, Gerhardt, & Mandelbaum, 2008).

Platelet-rich plasma therapy has been found in varied surgical fields to be able to enhance bone and soft tissue healing by placing autologous platelets at supra-physiological concentrations (Dhillon, Schwarz, & Maloney, 2012). For instance, increased bone activity and faster bone regeneration after using PRP were revealed by scintigraphy in dogs (Cho et al., 2013). In spite of a recent controversial finding reporting that PRP combined with bovine-derived xenograft may delay peri-implant bone healing in rabbits (Peng et al., 2016), there are also some in vitro animal experiments and preliminary clinical trials, which indicate that peri-implant sensory feedback may be modified and promoted by various growth factors released from autologous PRP (Huang et al., 2017).

Although the results from a recent systematic review suggested a positive effect of platelet concentrations on bone formation in clinical post-extraction sockets (Del Fabbro, Corbella, Taschieri, Francetti, & Weinstein, 2014), characterization of the healing and resulting bone structure with autologous PRP in physiological osseointegration of implants remains poorly documented or even controversial. Moreover, the influence of the concentration of platelet on the assumed development of peri-implant bone microstructures in a longer observation time has hardly been explored.

Traditional 2D histological techniques, previously regarded as the gold standard, can offer high-resolution imaging for understanding the hard or soft tissue and cellular reactions in the proximity of dental implants. However, 2D sections are highly dependent on the orientation and the placement of the section during histological processing, varying by 30% as reported in a comparative study (Sarve, Lindblad, Borgefors, & Johansson, 2011). 3D imaging modalities, by contrast, which is based on successive volumetric scan and reconstructions, can provide 3D bone structure and quantity information. Previous researches have presented the feasibility and reliability of using micro-CT or synchrotron micro-CT to analyze morphologic characteristics of trabecular or cortical bone across animal models and humans (Arvidsson, Sarve, & Johansson, 2015; Bonnet et al., 2009; Bouxsein et al., 2010; Hsu et al., 2016; Kampschulte et al., 2015; Van Dessel et al., 2016, 2017). Recently, with the help of a 2D-3D matching algorithm, a high level of agreement has been reported between histology and micro-CT techniques for bone areas as well as of bone-implant contact in corresponding slices (Becker, Stauber, Schwarz, & Beißbarth, 2015). Moreover, micro-CT (Cuijpers et al., 2015; Fang, Ding, Wang, & Zhu, 2014) and synchrotron micro-CT (Sarve et al., 2011, Arvidsson et al., 2015) were further employed to assess trabecular architectures around dental implants, which has also been validated by comparing with 2D histological way (Bissinger et al., 2017).

The purpose of the present study was to gain insights into how PRP at different concentrations may influence peri-implant trabecular bone volume and microarchitectures in a beagle dog model using high-resolution micro-CT. Additionally, the potential treatment benefits from PRP on osseointegration are discussed, along with an experimental setting integrating the biological data

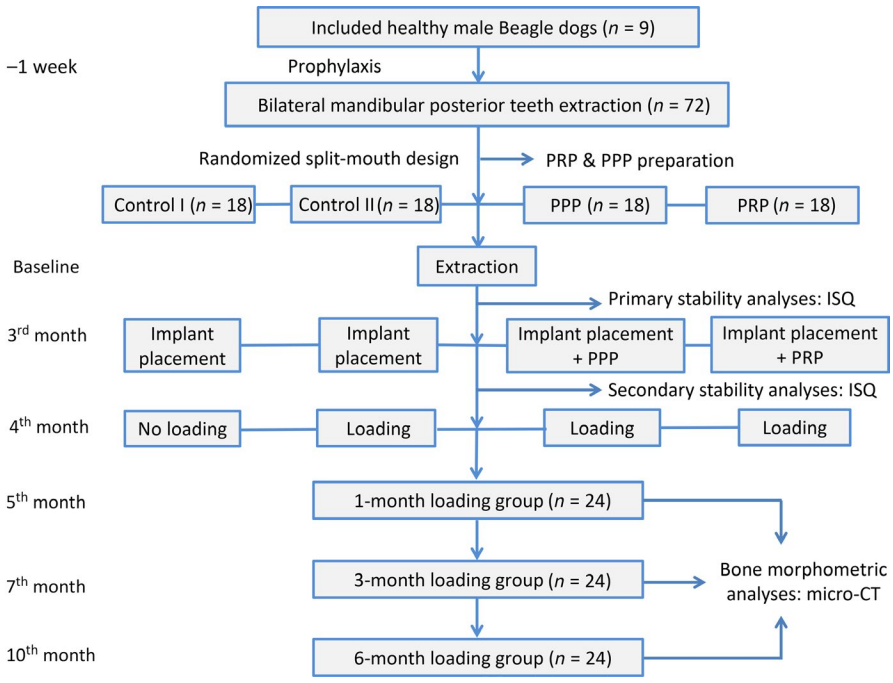

FIGURE 1 The time frame for the whole study design. Control I: implant placement without any loading; control II: implant placement with loading; PPP: platelet-poor plasma + implant placement with loading; and PRP: platelet-rich plasma + implant placement with loading

into our current understanding of mechanics of PRP and implant osseointegration.

2 | MATERIAL AND METHODS

2.1 | Study design

The protocol of this study was approved by the bioethics committee of West China College of Stomatology (WCCSIRB-D-2014-010). We carried out a split-mouth randomized study on 9 healthy male beagle dogs, by following the ARRIVE guidelines for preclinical animal studies (supplementary file, see http://www.equator-network.org/ for details). Sample size calculation was based on our previous study on dogs (Huang, Van Dessel, Depypere, et al., 2014; Huang, Van Dessel, Liang, et al., 2014). Before the experiment, there was one-week period to standardize feeding and environment factors on all dogs. The dogs were housed individually and fed according to the general feeding program at the Experimental Animal Center of State Key Laboratory of Biotherapy. The whole extraction and implant placements were performed by the same surgeon with a 6-year clinical experience in implant surgery, who was blinded to the allocation process during extraction but not to the later allocation of implant placements.

2.2 | Surgical procedure

Briefly, all 9 dogs (weighted 14.5–16.4 kg) received 1 week of antibiotics prophylaxis according to the previous experience of big animal experiment (Huang, Van Dessel, Liang, et al., 2014). Their posterior teeth, that is, 2nd-4th premolars and 1st molar, were then extracted at both lower jaws. After 1 month of healing, 8 commercially available dental implants with plasma-sprayed HA coating layer (3.3 mm Ø × 8 mm long, cylindrical, non-submerged healing, BLB, China) were placed in each dog at both sides of the mandible. The implants were placed with a controlled insertion torque ranging between 30 and 35 Ncm. All implants were randomly assigned to one of 4 groups (N = 18/group): implant placement without any loading (control I); implant placement with loading (control II); platelet-poor plasma placed into implant-recipient sites + implant placement with loading (PPP); and platelet-rich plasma placed into implant-recipient sites + implant placement with loading (PRP; Figure 1).

2.3 | PRP preparation and quantification of platelet concentration

According to the protocol adapted from a double-centrifugation way (Jo, Roh, Kim, Shin, & Yoon, 2013), blood (5 ml) was drawn from the dog before the breakfast and collected into a sterile syringe containing 1 ml of the anticoagulant sodium citrate. Then, the blood was centrifuged (Allegra × 30 R centrifuge, Beckman Coulter) at 700 g for 8 min. Next, the supernatant plasma and buffy coat were collected for a further condensation centrifugation at 1600 g for 8 min. Finally, the bottom of this buffy coat and supernatants was defined as PRP, while the top was further described as PPP (Figure 2). The concentration of platelet in the whole blood, PPP, and PRP was examined by a blood cell counter (KX-21NV, Sysmex).

2.4 | Occlusion restoration and resonance frequency analyses

During the experiment, the surgical conditions and occlusion restoration were kept same for all the groups. The implants were placed into the jawbone following a non-submerged and single-stage surgery, which allows its smooth neck part placed in the soft tissue while its HA coating part was just below the level of the marginal bone. Implant stability was confirmed by resonance frequency analyses (Osstell™; Integration Diagnostics). Specifically, the implant stability quotient (ISQ) values were recorded in both mesiodistal (MD) and buccolingual (BL) directions at the time of implant placement surgery (primary implant stability) and the time of post-crown restoration (secondary implant stability).

Customized posts with a resin crown (flowable resin composite under halogen light-curing unit for 20 s) were set by cement (3M ESPE). The edge-to-edge occlusion contacts while chewing was obtained at the most extent between the implant-recipient sites and antagonist teeth. During the whole experiment, the occlusal loading on each implant was kept similar, checking by using 20-μm articulating papers per month during the experiment (Accufilm II, RX, 3M ESPE). Plaque control was carefully applied once a week, by manually removing food residue and dental plaque with 0.2% chlorhexidine gel on top of a soft toothbrush.

2.5 | Animal sacrifice

The sacrifice was performed on three randomly selected dogs at each time point, namely 1, 3, and 6 months after implant placement surgery, respectively, with an overdose of xylazine hydrochloride (intravenous

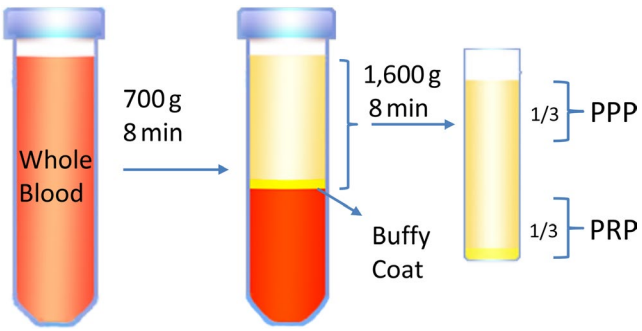

FIGURE 2 The process of platelet-poor plasma and platelet-rich plasma preparation. The fresh whole blood (5 ml) was drawn from the dogs before the breakfast and then centrifuged at 700 g for 8 min, resulting in three basic components: blood cells (bottom), buffy coat (middle), and plasma (top). Next, the supernatant plasma and buffy coat were collected for further preparation. Both components were centrifuged separately for a second time at 1600 g for 8 min. Both products were finally activated with 2% calcium chloride before experiment use

injection) and immediate perfusion of 4% paraformaldehyde and 0.0125% glutaraldehyde in 0.1 M phosphate buffer (pH 7.4). Specimen blocks (implants with about 4-mm peri-implant bone) were carefully retrieved and immediately immersed in the fixative Unifix® (4% formaldehyde, Tianjin Chemical Reagent Company) for 5 weeks at 4°C.

2.6 | Micro-CT analysis

In total, 72 bone sample blocks were scanned by high-resolution micro-CT (Quantum FX Caliper, Life Sciences, Perkin Elmer). The following exposure settings were kept same for each scanning: 20 μm voxel size, 360° rotation, 90 kV tube voltage, 160 microA tube current, 180 s scanning time, and a field of view (FOV) of 10 × 10 mm. The bone structural parameters were measured in three incremental cylindrical-shaped regions of interests (ROIs: 0.5, 1, and 1.5 mm W × 2 mm H) around the middle level of the implant. Briefly, before the selection of volume of interests (VOIs) from micro-CT, each implant was manually reoriented along its long axis in three-dimensional coordinates, respectively (i.e., axial, coronal, and sagittal planes) by using DataViewer (ver. 1.5.1.2, Bruker). Considering every implant has a standard length of 8 mm, the central region of the implant was set as 4 mm below from its cervical margin with a height of 2 mm. Next, the irregular anatomic regions were manually selected in each section through intermediate cross sections, in order to exclude the cortical bone in the cylindrical-shaped ROIs and keep only trabecular structures for the assessment (Figures 3 and 4). An adaptive threshold approach in CT-Analyser, also known as adaptive or local thresholding algorithms, has been applied to perform image segmentation (Figure 4). Standard 3D structural parameters of trabecular bone architecture were automatically quantified within the selected VOIs (Table 1), by using dedicated custom processing in the CTAn (version 1.16, CT-Analyser, Bruker; Huang, Van Dessel, Depypere, et al., 2014; Huang, Van Dessel, Liang, et al., 2014). One examiner was responsible for morphological analyses, who was blinded to the group allocation.

2.7 | Statistical analysis

One-way ANOVA and post hoc Tukey's HSD tests were used to compare variables between groups and time points (mean ± S.D.). Tukey's HSD test was used to compare variables between groups, and non-parametric multiple comparisons were applied when normality was not confirmed. Statistical analysis was performed in R 2.14.2 (R Development Core Team). The significance level α was 5% for all tests.

3 | RESULTS

All animals recovered well and without any clinical signs of inflammation during the experimental period, and all implants were clinically stable until euthanasia. The peri-implant bone and soft tissue were overall healthy.

3.1 | Platelet concentration in PRP and PPP

The platelet concentration examination was shown in Table 2. The average platelet concentration was the highest in PRP, with platelets almost fourfold higher than in whole blood, and about 150-fold higher than in PPP.

3.2 | Resonance frequency analyses

The primary and secondary implant stability results were recorded as ISQ values. As shown in Figure 5, the secondary implant stability in PPP and PRP groups increased significantly compared with their primary implant stability; however, there was no significant difference between these two groups. Although PPP and PRP had slightly lower primary stability than the control groups, no significant difference within four groups were observed for either primary or secondary stability.

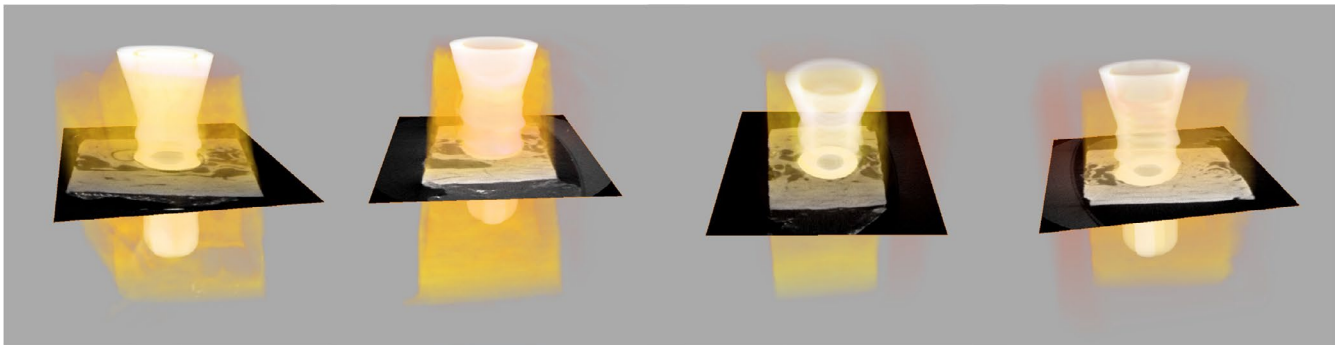

FIGURE 3 Three-dimensional surface reconstruction of the trabecular bone at the implant bone interface. Below images from left to right correspond to each group, respectively: control I: implant placement without any loading; control II: implant placement with loading; PPP: platelet-poor plasma + implant placement with loading; and PRP: platelet-rich plasma + implant placement with loading

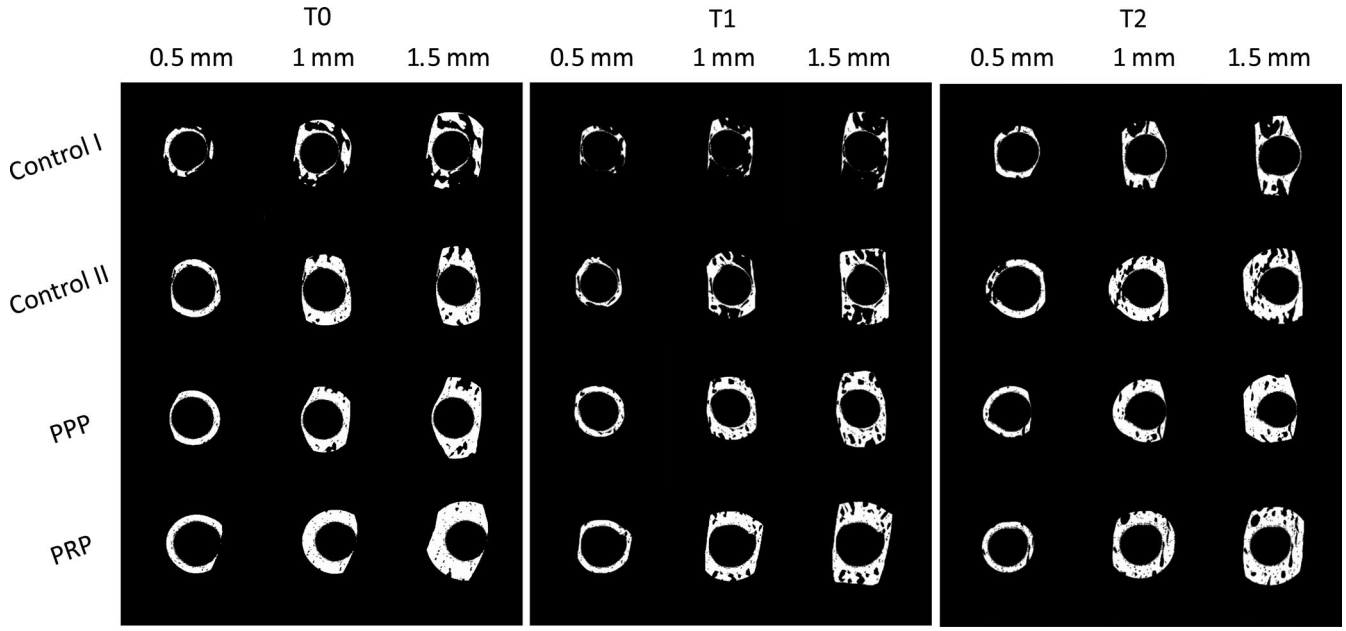

FIGURE 4 Morphometric evaluation (a custom processing was applied based on the thresholding segmentation) from micro-CT on peri-implant trabecular structures from four groups at radius of 0.5, 1, and 1.5 mm around the implant surface in each time point. To focus on the trabecular structures, the central and interproximal areas in each binary image, where the implant and the cortical bone, respectively, occupy, are both manually excluded from original micro-CT images. From left to right: T0, 1 month after implant placement and loading; T1, 3 months after implant placement and loading; and T2, 6 months after implant placement and loading

TABLE 1 Parameters quantified from micro-CT images for peri-implant bone morphometric evaluation in selected volumes of interest

Abbreviation	Morphologic parameters	Unit	Brief introduction
TV	Total volume of interest	(mm^3)	Volume of the entire region of interest
BV	Bone volume	(mm^3)	Volume of the region segmented as bone
BV/TV	Bone volume fraction	(%)	Ratio of the segmented bone volume to the total volume of the region of interest
Tb.Th	Trabecular thickness	(mm)	Mean thickness of trabeculae, analyzed using direct 3D methods
Tb.Sp	Trabecular separation	(mm)	Mean distance between trabeculae, analyzed using 3D methods
Po (tot)	Total porosity percentage	(%)	Ratio of the volume of all open plus closed pores to the total volume of interest

3.3 | Trabecular morphometric analyses

The reconstructed images displayed a high level of trabecular bone details, which showed the distinct structures of cortical and cancellous bone around titanium implants. The cancellous bone structure showed large, rod-like, connected trabeculae with round or oval voids in between. There were also some areas of incompletely matured bone with a disorganized structure composed of small, thin, and dense trabeculae similar to those of woven bone, which were mostly observed in the T0 and T1 time points (Figures 3 and 4).

As seen in Figure 6, in an area of 1 mm away from the implant surface, PPP and PRP groups had higher BV/TV (%, PPP-T0: 61.5 ± 7.8; PRP-T0: 66.0 ± 6.4; control II-T0: 55.1 ± 6.8; control I-T0: 41.0 ± 10.7; PPP-T1: 58.5 ± 16.7; PRP-T1: 59.6 ± 10.4; control II-T1: 47.6 ± 8.0; control I-T1: 39.1 ± 10.2; PPP-T2: 67.5 ± 6.0; PRP-T2: 72.9 ± 5.5; control II-T2: 55.9 ± 6.2; control I-T2: 45.2 ± 7.1) and Tb.Th (mm, PPP-T0: 0.23 ± 0.02; PRP-T0: 0.22 ± 0.02; control II-T0: 0.21 ± 0.01; control I-T0: 0.19 ± 0.01; PPP-T1: 0.23 ± 0.03; PRP-T1: 0.23 ± 0.02; control II-T1: 0.20 ± 0.02; control I-T1: 0.18 ± 0.01; PPP-T2: 0.24 ± 0.03; PRP-T2: 0.22 ± 0.03; control

TABLE 2 The average concentration of platelets in whole blood, PPP, and PRP (mean and *SD*, $\times 10^9$/L)

	Platelet ($\times 10^9$/L)	Significance
Whole blood (n = 6)	192.8 ± 24.2	–
PPP (n = 6)	4.8 ± 1.8	**
PRP (n = 6)	776.2 ± 144.0	***

Note: **, *** significant differences indicate, respectively, $p < .005$ and $p < .0001$ while comparing with whole blood samples.
Abbreviations: PPP, platelet-poor plasma; PRP, platelet-rich plasma.

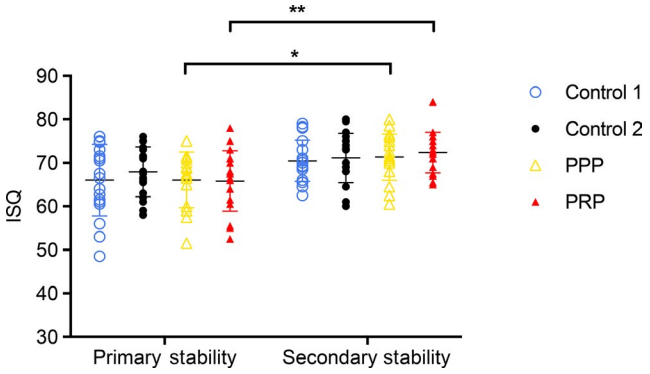

FIGURE 5 The primary and secondary implant stability evaluated by resonance frequency analyses. Each value was an average of four measurements from mesial, distal, buccal, and lingual directions. In the platelet-poor plasma and platelet-rich plasma groups, the secondary stability significantly increased compared with the primary stability before implant loading. *, ** significant differences indicate $p < .05$ and $p < .01$, respectively

II-T2: 0.20 ± 0.02; control I-T2: 0.19 ± 0.03) but lower Tb.Sp (mm, PPP-T0: 0.39 ± 0.14; PRP-T0: 0.35 ± 0.14; control II-T0: 0.49 ± 0.09; control I-T0: 0.51 ± 0.11; PPP-T1: 0.35 ± 0.05; PRP-T1: 0.34 ± 0.05; control II-T1: 0.47 ± 0.05; control I-T1: 0.51 ± 0.04; PPP-T2: 0.26 ± 0.05; PRP-T2: 0.22 ± 0.04; control II-T2: 0.45 ± 0.09; control I-T2: 0.58 ± 0.08) and Po (tot) (%, PPP-T0: 36.4 ± 5.6; PRP-T0: 34.1 ± 9.0; control II-T0: 48.7 ± 13.1; control I-T0: 60.0 ± 10.7; PPP-T1: 38.0 ± 12.8; PRP-T1: 38.0 ± 8.0; control II-T1: 55.6 ± 16.5; control I-T1: 63.4 ± 13.7; PPP-T2: 33.2 ± 5.6; PRP-T2: 28.4 ± 6.7; control II-T2: 51.3 ± 13.5; control I-T2: 67.4 ± 14.7) than the control groups for all 3 time points. In addition, the control groups had decreased BV/TV and Tb.Th after 3 months of healing, while this was not observed in both experimental groups. However, no distinct difference was found for all three time points between both experimental groups.

Moreover, as the investigated distance from the implant surface increased, there was no obvious change for BV/TV and Po (tot) within the same group and time point, yet Tb.Th and Tb.Sp continued to increase (Figure 7). The statistical differences were mainly observed among the areas of 0.5–1 mm and 1–1.5 mm away from implants.

4 | DISCUSSION

This study aimed to test the hypothesis that whether there is any difference in the peri-implant trabecular bone healing at different times with a different concentration of autologous PRP therapy. Although the biological graft has been clinically used for the last decade, there is not yet a straightforward conclusion concerning biological benefits of PRP on dental implants (Roffi et al., 2013). Besides, no specific information was reachable regarding trabeculae structures around implants, from the close to the distant. The current study was therefore designed, using high-resolution micro-CT, to investigate the performance of PRP at different concentrations on dental implants during a time frame of 6 months. In the following paragraphs, we address this knowledge gap and focus on how observations made in this study may be translated into clinically relevant information.

It is generally believed that the stability of the implant would increase steadily during the healing process. With the examination of secondary implant stability in our study, all groups confirmed a higher level of ISQ at 70 before the implant loading, which was over the critical limit of ISQ at 60 for a successful osseointegration (Gallucci et al., 2014). Beyond this, PPP and PRP had higher secondary stability (significant higher ISQ) than their primary stability, showing the initial biological effects of the autologous growth factors in PRP. Compared with control groups, there was only a trend that the PRP and PRP groups had lower primary stability. It is probably due to the addition of the autologous grafts, which acted as a buffering at the interface between implants and their surrounding bone. It seems that implant stability during the healing process especially increases for implants with lower primary or initial stabilities, which may serve as another evidence for the relationship of primary and secondary stability in dental implants (Miri, Khajavi, Shirzadeh, & Kermani, 2017).

The high-resolution micro-CT analyses in our study revealed that the PPP and PRP groups had an improved bone volume and structural parameters around implants (Van Dessel et al., 2016), as shown by increased BV/TV and Tb.Th and decreased Tb.Sp and Po (tot). The role of platelets within PRP in the wound healing process has so far been extensively reported, which are mediated by a pool of growth factors, such as platelet-derived growth factor (PDGF), vascular endothelial growth factor (VEGF), and transforming growth factor-β (TGF-β). These growth factors have shown their potentials to stimulate cell proliferation and differentiation (Badran, Abdallah, Torres, & Tamimi, 2018). The current results are consistent with some clinical findings (Gentile, Bottini, Spallone, Curcio, & Cervelli, 2010; Georgakopoulos et al., 2014), which indicate further that local application of PRP has positive effects on peri-implant trabecular bone remodeling in dental implant surgery, such as increased the numbers of osteogenic cells and faster rate of bone maturation, while the PPP could sufficiently maintain bone width and height with no depression for the preservation of socket with buccal dehiscence (Hatakeyama, Marukawa, Takahashi, & Omura, 2014).

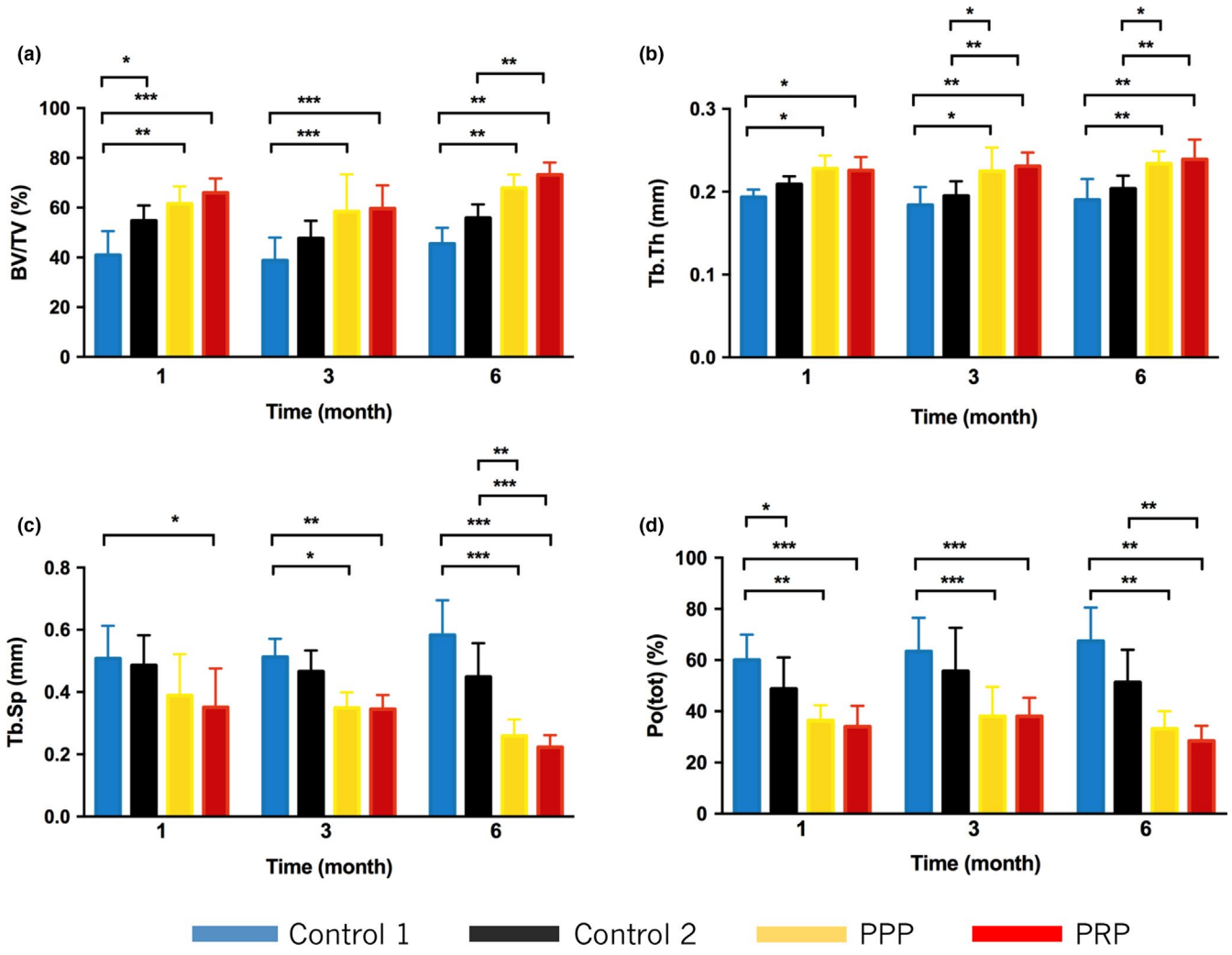

FIGURE 6 Comparison of 3D morphometric parameters (1mm of region of interest around implants) measured at the implant bone interface at the time point indicated. The micromorphology of the trabecular bone in the platelet-poor plasma (PPP) and platelet-rich plasma (PRP) groups was characterized by relatively higher values in BV/TV (a) and Tb.Th (b) but a lower value in Tb.Sp (c) and Po (tot) (d) in each observation time point. The micromorphology in the PPP group was similar to that of the PRP group at all observation time points. *, **, *** significant differences indicate $p < .05$, $p < .001$, and $p < .0001$, respectively

It is worth noting that the trabecular morphology in PPP group was similar to that of the PRP group at all observation time points. This finding suggests that autologous plasma products (PPP and PRP) are both capable to promote the trabecular bone volume and structure healing pattern, irrespective of whether or not the level of platelet is higher than the whole blood. It is likely that growth factors, as a fairly complex system, can stimulate the proliferation of any cells, no matter if the cells are involved in bone differentiation. As Tajima, Sotome, Marukawa, Omura, and Shinomiya (2007) reported, PRP not only promotes cell proliferation but also inhibits osteoblast differentiation of mesenchymal stem cells in a dose-dependent manner. Likewise, another animal study, where a rather similar PRP preparation protocol was used as in our study, found that the number of fibrin fibers in bundle form was greater in PPP than in PRP (Hatakeyama et al., 2014). It could be assumed that the final biological effects of PPP may be compensated by inherent greater fibrin fibers, despite its low level of platelets. All these studies imply that platelets and their growth factors, proteins, and cytokines within PRP make critical difference in peri-implant tissue regeneration (Huang et al., 2017); meanwhile, one should not ignore the fibrous insoluble fibrin inside the plasma products which serves as a kind scaffold for supporting cells and releasing growth factors.

Three-dimensional X-ray imaging ways, such as micro-CT and synchrotron micro-CT in preclinical and CBCT in clinical, have been applied to detect the trabecular structure and thus to quantify osseointegration at the interface of bone and implants, which already show their potentials in accuracy, reliability, and non-destructive than the traditional histological ways (Arvidsson et al., 2015; Becker et al., 2015; Corpas Ldos et al., 2011; Huang, Van Dessel, Depypere, et al., 2014; Muller et al., 1998). Routinely, bone regeneration is examined in a 500 μm zone from the implant surface either in a radiographic way (Cuijpers et al., 2014) or in a histological way (Romanos et al., 2003). By using a high-resolution micro-CT in the current study, we found that the bone structure parameters change

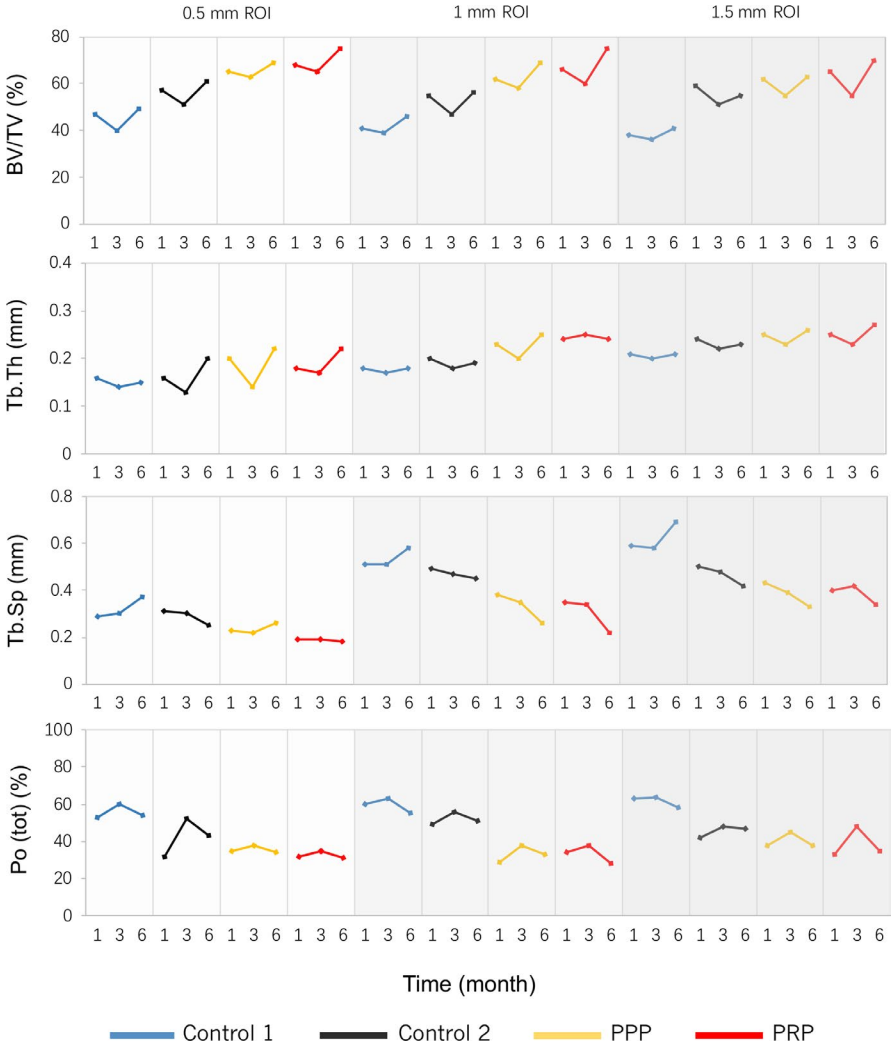

FIGURE 7 The bone structural parameters change accordingly with the distance from the implant. As the region of interest increases from 0.5 mm to 1.5 mm, BV/TV and Po (tot) remain unchanged while Tb.Th and Tb.Sp increase in all four groups during 1, 3, and 6 months

accordingly with the distance away from the implant. The more distance from the implant surface, especially from 1 mm to 1.5 mm, the better trabecular bone structures could be observed. This finding suggests that bone regeneration is more active nearby the implant surface, while peri-implant bone in more distant areas appears more mature, which is in accordance with another histomorphometric analysis (Cochran, 2006).

It should be recognized that, irradiating high density metallic implants is producing peri-implant image artifacts. With the application of micro-CT and adaptive thresholding in the current study, it is not yet possible to avoid all of this kind of artifact, mostly at the region adjacent to the implants. It is also known as beam-hardening effect that exists closely around implants in the reconstructed imaging, which could range from 45 μm to even 400 μm (Zou, Hunter, & Swain, 2011). Depending on the actual scanning configurations and the scanned metal material, artifacts may prevent a reliable discrimination between real mineralized tissues and metal implants. Hence to limit these possible metal artifacts as much as possible, scanning parameters, sample orientation, and reconstruction process in the micro-CT scanner were kept standard. In addition, reduced implant diameters were used in this study. Despite these parameters, special caution is indicated when evaluating the bone structure within a 200 μm radius around the surface of titanium implants (Li et al., 2014; Vandeweghe, Coelho, Vanhove, Wennerberg, & Jimbo, 2013). This is also one of the reasons why in this particular study three different ROIs, expending from 0.5 mm to 1.5 mm, were applied, thus ensuring an overall and objective image analysis. Additionally, synchrotron micro-CT is believed to produce more accurate tomographic reconstruction and higher resolution compared to traditional micro-CT. According to the recent study, it shows potential to have less beam-hardening artifacts around implants due to the parallel beam acquisition and higher signal-to-noise ratio in synchrotron micro-CT (Sarve et al., 2011).

The present study for the first time disclosed the effectiveness of PPP as well as PRP in peri-implant bone volume and structure remodeling, which fall in line with the usefulness of PPP in the preservation of sockets with buccal dehiscence (Hatakeyama et al., 2014). However, the optimum function condition of PPP and PRP for improving osseointegration and the interaction of growth factors within fibrin networks remains to be further investigated. The newly developed autologous plasma products (Badran et al., 2018), such as leukocyte- and platelet-rich fibrin (L-PRF) and concentrated growth factors (CGF), have been commercialized and applied in a number of

clinical application. It could be a further research direction to identify the inherent mechanism of these platelet concentrates, where the application of custom-made autologous growth factors may potentially contribute as an effective and reliable treatment in peri-implant bone regeneration.

Within the limitations of this preclinical study, the local application PRP around dental implants could reach the same level of stability of implants as controls, induce, and sustain peri-implant bone formation and their microarchitecture in a 6-month study period; moreover, the osteogenic response can be more efficaciously promoted from the close to the distant on the basis of high-resolution micro-CT assessment. Meanwhile, it is revealed that a fine-tuning of the PRP dose may not be necessary to optimize the balance of bone modeling around implants. Further studies are needed to elucidate the interactions between custom-made autologous growth factors and peri-implant bone regeneration.

ACKNOWLEDGEMENTS

The authors thank laboratory technicians from the Research Base of West China Hospital, Sichuan University, for their valuable help during the animal research. They received fellowship support from Research Foundation Flanders (FWO) from the Belgian government and Sichuan Province Science and Technology Support Program (2016SZ0010). Jeroen Van Dessel is a FWO research fellow (11.ZU.117N).

CONFLICT OF INTEREST

The authors declare that there was no conflict of interest in this study.

AUTHOR CONTRIBUTIONS

YH involved in manuscript draft, animal experiment, and design; ZKL performed imaging analyses and statistics; JVD involved in manuscript draft and discussion; BS performed manuscript finalize, micro-CT scanning, and technique support; BH carried out animal experiment, surgery, and design; IL carried out project application and discussion; CP carried out project support and discussion; RJ performed project design and corresponding. All authors involved in the paper writing and revising.

ORCID

Yan Huang https://orcid.org/0000-0003-2631-3016
Jeroen Van Dessel https://orcid.org/0000-0001-5084-8710
Benjamin Salmon https://orcid.org/0000-0001-8739-2753
Bo Huang https://orcid.org/0000-0002-1762-9812
Ivo Lambrichts https://orcid.org/0000-0001-7520-0021
Constantinus Politis https://orcid.org/0000-0003-4772-9897
Reinhilde Jacobs https://orcid.org/0000-0002-3461-0363

REFERENCES

Arvidsson, A., Sarve, H., & Johansson, C. B. (2015). Comparing and visualizing titanium implant integration in rat bone using 2D and 3D techniques. *Journal of Biomedical Materials Research Part B: Applied Biomaterials*, *103*(1), 12–20. https://doi.org/10.1002/jbm.b.33168

Badran, Z., Abdallah, M. N., Torres, J., & Tamimi, F. (2018). Platelet concentrates for bone regeneration: Current evidence and future challenges. *Platelets*, *29*(2), 105–112. https://doi.org/10.1080/09537104.2017.1327656

Becker, K., Stauber, M., Schwarz, F., & Beißbarth, T. (2015). Automated 3D–2D registration of X-ray microcomputed tomography with histological sections for dental implants in bone using chamfer matching and simulated annealing. *Computerized Medical Imaging and Graphics*, *44*, 62–68. https://doi.org/10.1016/j.compmedimag.2015.04.005

Bissinger, O., Probst, F. A., Wolff, K. D., Jeschke, A., Weitz, J., Deppe, H., & Kolk, A. (2017). Comparative 3D micro-CT and 2D histomorphometry analysis of dental implant osseointegration in the maxilla of minipigs. *Journal of Clinical Periodontology*, *44*(4), 418–427. https://doi.org/10.1111/jcpe.12693

Bonnet, N., Laroche, N., Vico, L., Dolleans, E., Courteix, D., & Benhamou, C. L. (2009). Assessment of trabecular bone microarchitecture by two different x-ray microcomputed tomographs: A comparative study of the rat distal tibia using Skyscan and Scanco devices. *Medical Physics*, *36*(4), 1286–1297. https://doi.org/10.1118/1.3096605

Bouxsein, M. L., Boyd, S. K., Christiansen, B. A., Guldberg, R. E., Jepsen, K. J., & Muller, R. (2010). Guidelines for assessment of bone microstructure in rodents using micro–computed tomography. *Journal of Bone and Mineral Research*, *25*(7), 1468–1486. https://doi.org/10.1002/jbmr.141

Buser, D., Sennerby, L., & De Bruyn, H. (2017). Modern implant dentistry based on osseointegration: 50 years of progress, current trends and open questions. *Periodontology 2000*, *73*(1), 7–21. https://doi.org/10.1111/prd.12185

Cho, K., Kim, J. M., Kim, M. H., Kang, S. S., Kim, G., & Choi, S. H. (2013). Scintigraphic evaluation of osseointegrative response around calcium phosphate-coated titanium implants in tibia bone: Effect of platelet-rich plasma on bone healing in dogs. *European Surgical Research*, *51*(3-4), 138–145. https://doi.org/10.1159/000357197

Cochran, D. L. (2006). The evidence for immediate loading of implants. *Journal of Evidence Based Dental Practice*, *6*(2), 155–163. https://doi.org/10.1016/j.jebdp.2006.04.018

Corpas Ldos, S., Jacobs, R., Quirynen, M., Huang, Y., Naert, I., & Duyck, J. (2011). Peri-implant bone tissue assessment by comparing the outcome of intra-oral radiograph and cone beam computed tomography analyses to the histological standard. *Clinical Oral Implants Research*, *22*(5), 492–499. https://doi.org/10.1111/j.1600-0501.2010.02029.x

Cuijpers, V. M., Alghamdi, H. S., Van Dijk, N. W., Jaroszewicz, J., Walboomers, X. F., & Jansen, J. A. (2015). Osteogenesis around CaP-coated titanium implants visualized using 3D histology and micro-computed tomography. *Journal of Biomedical Materials Research Part A*, *103*(11), 3463–3473. https://doi.org/10.1002/jbm.a.35485

Cuijpers, V. M. J. I., Jaroszewicz, J., Anil, S., Al Farraj Aldosari, A., Walboomers, X. F., & Jansen, J. A. (2014). Resolution, sensitivity, and in vivo application of high-resolution computed tomography for titanium-coated polymethyl methacrylate (PMMA) dental implants. *Clinical Oral Implants Research*, *25*(3), 359–365. https://doi.org/10.1111/clr.12128

Del Fabbro, M., Corbella, S., Taschieri, S., Francetti, L., & Weinstein, R. (2014). Autologous platelet concentrate for post-extraction socket healing: A systematic review. *European Journal of Oral Implantology*, *7*(4), 333–344.

Dhillon, R. S., Schwarz, E. M., & Maloney, M. D. (2012). Platelet-rich plasma therapy - future or trend? *Arthritis Research & Therapy*, *14*(4), 219. https://doi.org/10.1186/ar3914

Fang, L., Ding, X., Wang, H. M., & Zhu, X. H. (2014). Chronological changes in the microstructure of bone during peri-implant healing: A microcomputed tomographic evaluation. *British Journal of Oral and Maxillofacial Surgery*, *52*(9), 816–821. https://doi.org/10.1016/j.bjoms.2014.07.097

Gallucci, G. O., Benic, G. I., Eckert, S. E., Papaspyridakos, P., Schimmel, M., Schrott, A., & Weber, H. P. (2014). Consensus statements and clinical recommendations for implant loading protocols. *The International Journal of Oral & Maxillofacial Implants*, *29*, 287–290. https://doi.org/10.11607/jomi.2013.g4

Gentile, P., Bottini, D. J., Spallone, D., Curcio, B. C., & Cervelli, V. (2010). Application of platelet-rich plasma in maxillofacial surgery: Clinical evaluation. *Journal of Craniofacial Surgery*, *21*(3), 900–904. https://doi.org/10.1097/SCS.0b013e3181d878e9

Georgakopoulos, I., Tsantis, S., Georgakopoulos, P., Korfiatis, P., Fanti, E., Martelli, M., & Martelli, F. S. (2014). The impact of platelet rich plasma (PRP) in osseointegration of oral implants in dental panoramic radiography: Texture based evaluation. *Clinical Cases in Mineral and Bone Metabolism*, *11*(1), 59–66. https://doi.org/10.11138/ccmbm/2014.11.1.059

Hatakeyama, I., Marukawa, E., Takahashi, Y., & Omura, K. (2014). Effects of platelet-poor plasma, platelet-rich plasma, and platelet-rich fibrin on healing of extraction sockets with buccal dehiscence in dogs. *Tissue Engineering Part A*, 874–882. https://doi.org/10.1089/ten.tea.2013.0058

Hsu, P. Y., Tsai, M. T., Wang, S. P., Chen, Y. J., Wu, J., & Hsu, J. T. (2016). Cortical bone morphological and trabecular bone microarchitectural changes in the mandible and femoral neck of ovariectomized rats. *PLoS ONE*, *11*(4), e0154367. https://doi.org/10.1371/journal.pone.0154367

Huang, Y., Bornstein, M. M., Lambrichts, I., Yu, H. Y., Politis, C., & Jacobs, R. (2017). Platelet-rich plasma for regeneration of neural feedback pathways around dental implants: A concise review and outlook on future possibilities. *International Journal of Oral Science*, *9*(1), 1–9. https://doi.org/10.1038/ijos.2017.1

Huang, Y., Van Dessel, J., Depypere, M., EzEldeen, M., Iliescu, A. A., Santos, E. D., & Jacobs, R. (2014). Validating cone-beam computed tomography for peri-implant bone morphometric analysis. *Bone Res*, *2*, 14010. https://doi.org/10.1038/boneres.2014.10

Huang, Y., Van Dessel, J., Liang, X., Depypere, M., Zhong, W., Ma, G., & Jacobs, R. (2014). Effects of immediate and delayed loading on peri-implant trabecular structures: A cone beam CT evaluation. *Clinical Implant Dentistry and Related Research*, *16*(6), 873–883. https://doi.org/10.1111/cid.12063

Jo, C. H., Roh, Y. H., Kim, J. E., Shin, S., & Yoon, K. S. (2013). Optimizing platelet-rich plasma gel formation by varying time and gravitational forces during centrifugation. *Journal of Oral Implantology*, *39*(5), 525–532. https://doi.org/10.1563/AAID-JOI-D-10-00155

Kampschulte, M., Erdmann, G., Sender, J., Martels, G., Bocker, W., ElKhassawna, T., & Krombach, G. A. (2015). The development and validation of micro-CT of large deep frozen specimens. *Scanning*, *37*(1), 63–72. https://doi.org/10.1002/sca.21180

Li, J. Y., Pow, E. H., Zheng, L. W., Ma, L., Kwong, D. L., & Cheung, L. K. (2014). Quantitative analysis of titanium-induced artifacts and correlated factors during micro-CT scanning. *Clinical Oral Implants Research*, *25*(4), 506–510. https://doi.org/10.1111/clr.12200

Miri, R., Khajavi, A., Shirzadeh, A., & Kermani, H. (2017). Relationship and changes of primary and secondary stability in dental implants: A review. *International Journal of Contemporary Dental and Medical Reviews*, *2017*, 6. https://doi.org/10.15713/ins.ijcdmr.112

Muller, R., Van Campenhout, H., Van Damme, B., Van Der Perre, G., Dequeker, J., Hildebrand, T., & Ruegsegger, P. (1998). Morphometric analysis of human bone biopsies: A quantitative structural comparison of histological sections and micro-computed tomography. *Bone*, *23*(1), 59–66. https://doi.org/10.1016/S8756-3282(98)00068-4

Peng, W., Kim, I. K., Cho, H. Y., Seo, J. H., Lee, D. H., Jang, J. M., & Park, S. H. (2016). The healing effect of platelet-rich plasma on xenograft in peri-implant bone defects in rabbits. *Maxillofacial Plastic and Reconstructive Surgery*, *38*(1), 16. https://doi.org/10.1186/s40902-016-0061-5

Roffi, A., Filardo, G., Elizaveta, K., & Marcacci, M. (2013). Does PRP enhance bone integration with grafts, graft substitutes, or implants? A systematic review. *BMC Musculoskeletal Disorders*, *14*, 330. https://doi.org/10.1186/1471-2474-14-330

Romanos, G. E., Toh, C. G., Siar, C. H., Wicht, H., Yacoob, H., & Nentwig, G. H. (2003). Bone-implant interface around titanium implants under different loading conditions: A histomorphometrical analysis in the Macaca fascicularis monkey. *Journal of Periodontology*, *74*(10), 1483–1490. https://doi.org/10.1902/jop.2003.74.10.1483

Sampson, S., Gerhardt, M., & Mandelbaum, B. (2008). Platelet rich plasma injection grafts for musculoskeletal injuries: A review. *Current Reviews in Musculoskeletal Medicine*, *1*(3-4), 165–174. https://doi.org/10.1007/s12178-008-9032-5

Sarve, H., Lindblad, J., Borgefors, G., & Johansson, C. B. (2011). Extracting 3D information on bone remodeling in the proximity of titanium implants in SRμCT image volumes. *Computer Methods and Programs in Biomedicine*, *102*(1), 25–34. https://doi.org/10.1016/j.cmpb.2010.12.011

Tajima, N., Sotome, S., Marukawa, E., Omura, K., & Shinomiya, K. (2007). A three-dimensional cell-loading system using autologous plasma loaded into a porous β-tricalcium-phosphate block promotes bone formation at extraskeletal sites in rats. *Materials Science and Engineering: C*, *27*(4), 625–632. https://doi.org/10.1016/j.msec.2006.05.031

Van Dessel, J., Nicolielo, L. F., Huang, Y., Coudyzer, W., Salmon, B., Lambrichts, I., & Jacobs, R. (2017). Accuracy and reliability of different cone beam computed tomography (CBCT) devices for structural analysis of alveolar bone in comparison with multislice CT and micro-CT. *European Journal of Oral Implantology*, *10*(1), 95–105.

Van Dessel, J., Nicolielo, L. F., Huang, Y., Slagmolen, P., Politis, C., Lambrichts, I., & Jacobs, R. (2016). Quantification of bone quality using different cone beam computed tomography devices: Accuracy assessment for edentulous human mandibles. *European Journal of Oral Implantology*, *9*(4), 411–424.

Vandeweghe, S., Coelho, P. G., Vanhove, C., Wennerberg, A., & Jimbo, R. (2013). Utilizing micro-computed tomography to evaluate bone structure surrounding dental implants: A comparison with histomorphometry. *Journal of Biomedical Materials Research Part B: Applied Biomaterials*, *101*(7), 1259–1266. https://doi.org/10.1002/jbm.b.32938

Zou, W., Hunter, N., & Swain, M. V. (2011). Application of polychromatic microCT for mineral density determination. *Journal of Dental Research*, *90*(1), 18–30. https://doi.org/10.1177/0022034510378429

SUPPORTING INFORMATION

Additional supporting information may be found online in the Supporting Information section at the end of the article.

How to cite this article: Huang Y, Li Z, Van Dessel J, et al. Effect of platelet-rich plasma on peri-implant trabecular bone volume and architecture: A preclinical micro-CT study in beagle dogs. *Clin Oral Impl Res*. 2019;30:1190–1199. https://doi.org/10.1111/clr.13532